

Time-Reversal Invariance and the Relation between Wave Chaos and Classical Chaos

Roel Snieder

Department of Geophysics and Center for Wave Phenomena,
Colorado School of Mines, Golden/Colo./CO/ 80401-1887, USA
rsnieder@mines.edu

Abstract. Many imaging techniques depend on the fact that the waves used for imaging are invariant for time reversal. The physical reason for this is that in imaging one propagates the recorded waves backward in time to the place and time when the waves interacted with the medium. In this chapter, the invariance for time reversal is shown for Newton's law, Maxwell's equations, the Schrödinger equation and the equations of fluid mechanics. The invariance for time reversal can be used as a diagnostic tool to study the stability of the temporal evolution of systems. This is used to study the relation between classical chaos and wave chaos, which also has implications for quantum chaos. The main conclusion is that in classical chaos perturbations in the system grow exponentially in time [$\exp(\mu t)$], whereas for the corresponding wave system perturbations grow at a much smaller rate algebraically with time (\sqrt{t}).

1 Time-Reversal Invariance of the Laws of Nature

Most laws of nature are invariant for time reversal. The only exceptions are the weak force that governs radioactive decay and equations that describe statistical properties such as the heat equation. This means that when we let the clock run backwards rather than forwards, the deterministic laws that govern the macroscopic world do not change. Mathematically, time reversal implies that the time t is replaced by $-t$. By making the substitution $t \rightarrow -t$ and by verifying whether the equation under consideration changes, one can verify whether the physical law is unchanged under time reversal.

As a first example let us consider Newton's third law which governs the motion of bodies in classical mechanics:

$$m \frac{d^2 \mathbf{r}}{dt^2} = \mathbf{F}(\mathbf{r}) . \quad (1)$$

In this expression \mathbf{F} denotes the force that acts on a particle with mass m at location \mathbf{r} . Under the substitution $t \rightarrow -t$, Newton's law does not change because the second time derivative is insensitive to the multiplication with the factor $(-1)^2$ that follows from this substitution. Mathematically this can be expressed by stating that Newton's law transforms as $m d^2 \mathbf{r} / dt^2 = \mathbf{F}(\mathbf{r}) \rightarrow m d^2 \mathbf{r} / d(-t)^2 = \mathbf{F}(\mathbf{r})$, which is identical to the original law (1). This means that when $\mathbf{r}(t)$ is a solution, then so is $\mathbf{r}(-t)$. Physically this means that

when a particle follows a trajectory then when one reverses the velocity of the particle at one point it will retrace its original trajectory.

Pressure waves in an acoustic medium satisfy the acoustic wave equation:

$$\rho \nabla \cdot \left(\frac{1}{\rho} \nabla p \right) - \frac{1}{c^2} \frac{\partial^2 p}{\partial t^2} = 0. \quad (2)$$

Because of the invariance of the second time derivative under time reversal, pressure waves in an acoustic medium are invariant for time reversal as well. This means that when $p(\mathbf{r}, t)$ is a solution then the time-reversed wavefield $p(\mathbf{r}, -t)$ is also a solution.

At this point you may think that the invariance for time reversal is due to the occurrence of the second time derivative in the equations. This is not necessarily the case. In classical electromagnetism the electric field \mathbf{E} and the magnetic field \mathbf{B} obey in vacuum Maxwell's equations, which contain only the first time derivative:

$$\begin{aligned} \nabla \cdot \mathbf{E} &= 4\pi\rho/\varepsilon_0 & , & & \mu_0 \nabla \times \mathbf{B} - \frac{\varepsilon_0}{c} \frac{\partial \mathbf{E}}{\partial t} &= \frac{4\pi}{c} \mathbf{J} , \\ \nabla \cdot \mathbf{B} &= 0 & , & & \nabla \times \mathbf{E} + \frac{1}{c} \frac{\partial \mathbf{B}}{\partial t} &= 0 . \end{aligned} \quad (3)$$

In this expression ρ is the charge density, \mathbf{J} is the electrical current density, ε_0 is the electrical permittivity and μ_0 is the magnetic susceptibility. Under time reversal ($t \rightarrow -t$) Maxwell's equations transform to

$$\begin{aligned} \nabla \cdot \mathbf{E} &= 4\pi\rho/\varepsilon_0 & , & & \mu_0 \nabla \times (-\mathbf{B}) - \frac{\varepsilon_0}{c} \frac{\partial \mathbf{E}}{\partial(-t)} &= \frac{4\pi}{c} (-\mathbf{J}) , \\ \nabla \cdot (-\mathbf{B}) &= 0 & , & & \nabla \times \mathbf{E} + \frac{1}{c} \frac{\partial(-\mathbf{B})}{\partial(-t)} &= 0 . \end{aligned} \quad (4)$$

Note that these expressions are identical to the original Maxwell's equations (3) with the exception that the magnetic field \mathbf{B} and the current \mathbf{J} have changed sign. This is due to the fact that when one changes the direction of time the velocity of the charges changes sign; hence the associated current changes sign as well: $\mathbf{J} \rightarrow -\mathbf{J}$. Since the electric current is the source of the magnetic field, the magnetic field therefore also changes sign under time reversal ($\mathbf{B} \rightarrow -\mathbf{B}$). However, the Lorentz force $\mathbf{F} = q(\mathbf{E} + \mathbf{v} \times \mathbf{B})$ does *not* change sign because under time reversal both the magnetic field \mathbf{B} and the velocity \mathbf{v} change sign. This means that under time reversal the magnetic field \mathbf{B} is not invariant because it changes sign. However, the functional form of the transformed equations (4) and the original equations (3) is identical and the imprint of the associated fields on charges is unaffected because the Lorentz force does not change under time reversal. For this reason one can state that the laws of classical electromagnetism are invariant under time reversal.

In quantum mechanics the wave-character of a particle is described by Schrödinger's equation:

$$i\hbar \frac{\partial \psi}{\partial t} = -\frac{\hbar^2}{2m} \nabla^2 \psi + V\psi, \quad (5)$$

where $V(\mathbf{r})$ denotes a real potential. When t is replaced by $-t$ and when one takes the complex conjugate, this equation transforms to

$$(-i)\hbar \frac{\partial \psi^*}{\partial (-t)} = -\frac{\hbar^2}{2m} \nabla^2 \psi^* + V\psi^*. \quad (6)$$

This equation is identical to (5) because the minus signs in the first term cancel each other. This implies that when $\psi(\mathbf{r}, t)$ is a solution of Schrödinger's equation, then $\psi^*(\mathbf{r}, -t)$ is a solution as well. Since in quantum mechanics only the absolute value $|\psi|^2$ leads to observable effects, one can state that the Schrödinger equation is invariant for time reversal.¹

The time-reversal invariance of Maxwell's equations is related to the fact that the current and the magnetic field reverse sign under time reversal. From this you may have concluded that time-reversal invariance only holds for linear equations. To show that this is not true, we consider as a last example a fluid that is exposed to a body force \mathbf{F} . The equation of motion is given by

$$\rho \frac{\partial \mathbf{v}}{\partial t} + \rho \mathbf{v} \cdot \nabla \mathbf{v} = \mathbf{F}. \quad (7)$$

Under time reversal, $t \rightarrow -t$, the velocity changes sign because $\mathbf{v} = d\mathbf{r}/dt \rightarrow d\mathbf{r}/d(-t) = -\mathbf{v}$, so that this expression changes under time reversal to

$$\rho \frac{\partial (-\mathbf{v})}{\partial (-t)} + \rho (-\mathbf{v}) \cdot \nabla (-\mathbf{v}) = \mathbf{F}. \quad (8)$$

This expression is identical to the original expression (7) because the minus signs cancel. This implies that when $\mathbf{v}(\mathbf{r}, t)$ is a solution of the equation of motion of the fluid, then $-\mathbf{v}(\mathbf{r}, -t)$ is a solution as well. This has been demonstrated in a beautiful experiment by *Chaiken et al.* [1], who mixed white paint through black paint by rotating a cylinder in the paint. When the cylinder was rotated in the reverse direction the paint "un-mixed" again and the white paint contracted to a localized blob in the black paint.

It should be noted that when one adds dissipation to the equation, the invariance for time reversal is lost. For example, when viscosity is added to expression (7), this expression changes to $\rho \partial \mathbf{v} / \partial t + \rho \mathbf{v} \cdot \nabla \mathbf{v} = \mu \nabla^2 \mathbf{v} + \mathbf{F}$. Under time reversal this expression transforms to $\rho \partial (-\mathbf{v}) / \partial (-t) + \rho (-\mathbf{v}) \cdot \nabla (-\mathbf{v}) =$

¹ This is in fact a slight over-simplification. In quantum mechanics the expectation value of Hermitian operators are the only observable quantities. One can show that for such an operator the expectation value does not change when one takes the complex conjugate of the wavefunction ψ .

$\mu \nabla^2 (-\mathbf{v}) + \mathbf{F}$, which is *not* identical to the original expression because the viscous term $\mu \nabla^2 \mathbf{v}$ changes sign. In general, dissipation implies a direction of time because energy is lost from the system (with time). Therefore, invariance for time reversal can only be expected in the absence of dissipation.

The results of this section imply that in the absence of dissipation the laws of classical mechanics, acoustic wave propagation, classical electromagnetism, quantum mechanics, and fluid mechanics are invariant under time reversal. Yet in our daily life we clearly experience a “direction” of time. When a vase falls on the floor we see it break and all the parts fly around, yet we never see pieces of pottery suddenly assemble themselves to a vase which then flies upward in the air. With the years our body ages, the phrase “growing older” encapsulates a notion that time moves in one direction. The fact that the basic natural laws are invariant for time reversal, but that we clearly experience a direction of time, is called the paradox of the “arrow of time” [2]. Detailed accounts of this issue are given by *Coveny* and *Highfield* [3] and by *Price* [4].

The invariance of the basic equations in physics for time reversal forms the basis of many applications that are described in this book where waves are re-emitted from receivers so that they propagate back to the original source. A clear example is given by *Derode et al.* [5], who propagated acoustic waves through a dense assemblage of scatterers to an array of receivers. The recorded signals are digitized and then time-reversed in a computer after which they are re-emitted from the receivers. These waves focus after a certain time at the original source. This process of time-reversed propagation is very stable to errors in re-emitted signal [6]. The stability of the back-propagation of strongly scattered waves to the addition of random noise is explained by *Scales* and *Snieder* [7].

2 Wave Chaos and Particle Chaos

At the end of the 19th century, scientists saw the universe as a clockwork that obeyed the laws of classical physics. If one would know the initial position and initial velocity of all the particles, one could predict the future evolution of the universe with great accuracy. Quantum mechanics shattered this mechanistic dream (or nightmare?) because chance or probability forms an integral part of this theory. In the 20th century it became apparent that very simple dynamical systems showed such a strong sensitive dependence on perturbations in the initial conditions that the prediction of the temporal evolution of such a system is practically impossible. A famous example is the Lorenz system which accounts for the air flow in a simplified model for the atmosphere [8]. In chaotic dynamical systems the perturbations in the solutions grow exponentially with time [$\exp(\mu t)$] so that errors in the initial condition quickly lead to a very different solution. The factor μ is called the *Lyapunov exponent*. A detailed and clear account of classical chaos is given by *Tabor* [9].

Suppose one has a system where the classical equations of motion lead to chaotic behavior. How does the corresponding wave system then behave? This question is highly relevant because quantum mechanics is the wave extension of classical mechanics, and one may wonder how the solution of the Schrödinger equation behaves under a perturbation of the system that for the classical system leads to chaos. This has led to the formulation of “quantum chaos” [9]. It is not obvious that the wave system shows the same dependence to perturbations of the system as the classical system, because waves carry out a natural smoothing [10,11]. The finite extent of the wave field ensures that a wave samples space in a more extended way than a particle. This smoothing effect could render wave propagation much more stable for perturbations of the system than particle propagation [12].

In this chapter the stability of wave propagation is not addressed with solutions of the Schrödinger equation, but with a numerical simulation of waves that are analogous to the acoustic waves used in the experiments of *Derode et al.* [5]. The geometry of the system is shown in Fig. 1. A numerical simulation of the experiment of *Derode et al.* [5] is well suited to study the stability of the propagation of waves or particles to perturbations. The idea is that waves (or particles) propagate from a source through the system and are recorded at receivers. The system is then perturbed, and the waves (or particles) are re-emitted backward in time from the receivers. Because of the invariance of the system for time reversal, the waves (or particles) should converge back onto the source at time $t = 0$. When the system is perturbed, this focussing of waves (or particles) onto the original source position is degraded. This degradation of the focusing on the source position can be used as a measure of the sensitivity of system to perturbations.

In the numerical experiment waves or particles are emitted from a source and then propagate through an assemblage of isotropic point scatterers. In the wave experiments the waves are recorded on 96 equidistant receivers on the

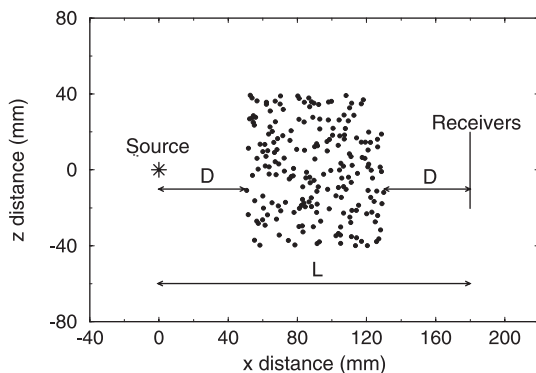


Fig. 1. Geometry of the numerical experiment with time-reversed propagation. Dots: scatterers

line marked “receivers.” For the particles a particle is detected when it crosses the receiver line. For the time-reversed particle propagation the velocity of the particle at the receiver location is reversed, and the particle is re-emitted at time $-t$ towards the scatterers. For the time-reversed propagation of the waves the recorded wave field is numerically time-reversed and re-emitted from the receivers. It should be noted that the particles do not interact with each other, they are only scattered by the scatterers of the system.

In order to make a fair comparison, the isotropic point scatterers have the same cross-section for the waves and the particle simulation. The numerical values of the parameters are shown in Table 1. For these parameters the system can be considered to be a strongly scattering system because the size of the scatterer array (approximately 80 mm) is much larger than the mean free path (15.56 mm). As discussed by *Scales* and *Snieder* [13] such strongly scattered waves show aspects of diffusive behavior.

It should be noted that the equations of particle propagation in classical mechanics are formally equivalent to the equation of kinematic ray-tracing that governs the trajectories of rays. Therefore the comparison between wave propagation and particle propagation not only has a bearing on the relation between classical chaos and quantum chaos, it is also relevant for the relation between ray-geometric solutions and full-wave solutions.

Table 1. Numerical values of parameters in numerical experiment

Symbol	Property	Value
σ	Scattering cross-section	1.592 mm
l	Mean free path	15.56 mm
λ	Dominant wavelength	2.5 mm

3 Instability of Particle Trajectories

In this section the stability properties of particle trajectories are treated. A full derivation of the results presented in this section and the next can be found in *Snieder* and *Scales* [14] and in *Snieder* [15]. It is shown in these references that when a trajectory has the initial perturbation Δ_{in} the perturbation after n scattering events is on average given by

$$\Delta_{\text{out}} = \left(\frac{2\pi l}{\sigma} \right)^n \Delta_{\text{in}}, \quad (9)$$

where l is the mean free path and σ is the scattering cross-section. On average, a particle encounters a scatterer after each time interval l/v , where v is the velocity of the particle. This means that after a time t the number of encountered scatterers is on average given by

$$n = \frac{vt}{l}. \quad (10)$$

Using this in (9) one finds that the perturbation $\Delta(t)$ in trajectories grows exponentially with time:

$$\Delta(t) = e^{\mu t} \Delta(0), \quad (11)$$

where the Lyapunov coefficient μ is given by

$$\mu = \frac{v}{l} \ln \left(\frac{2\pi l}{\sigma} \right). \quad (12)$$

This implies that perturbations in the trajectories grow exponentially with time, which is one of the characteristics of chaotic behavior.

When the growth in the perturbation of a trajectory is comparable to the cross-section σ of the scatterers, a particle may suddenly miss a scatterer that it encountered on its unperturbed trajectory. Under this condition the particle will follow a fundamentally different trajectory. The associated critical length scale for the perturbation of the scatterer positions is derived by *Sniieder* and *Scales* [14] and is given by

$$\delta_c^{\text{part}} = \left(\frac{\sigma}{2\pi l} \right)^n \frac{\sigma}{2}. \quad (13)$$

Using (10) and (12) one finds that this critical length scale decreases *exponentially* with time:

$$\delta_c^{\text{part}} = \frac{\sigma}{2} e^{-\mu t}. \quad (14)$$

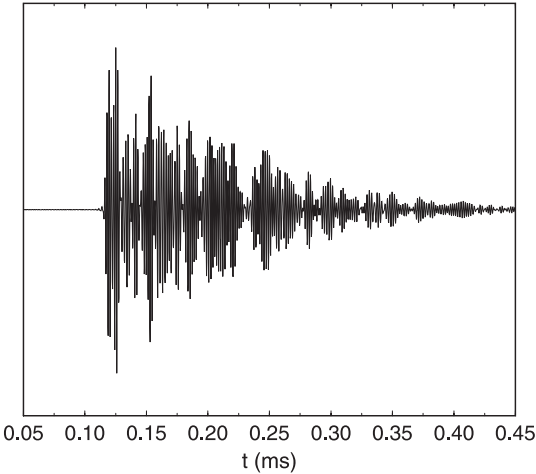
Equation (13) states that the critical length scale is proportional to the cross-section σ multiplied by the dimensionless number $(\sigma/2\pi l)^n$. Since for the employed parameter setting the mean-free path l is much larger than the scattering cross-section σ (see Table 1), the critical length scale decreases dramatically as a function of the number of scatterers encountered (see Table 2). Note that even for a limited number of scatterer encounters n the critical length scale becomes much smaller than any of the characteristic dimensions of the system (which are all of the order of millimeters).

4 Instability of Wave Propagation

The wave field that propagates through a system of isotropic scatterers can be computed in a relatively simple way using the method of *Groenenboom* and *Sniieder* [10], which is described in great detail by *Sniieder* [15]. The wave field recorded at a receiver in the middle of the receiver array is shown in Fig. 2. The wave field consists of a long extended wave train of multiply scattered waves. This is a result of the fact that the mean free path is much less than the propagation distance of the waves (see Table 1).

Table 2. Critical error δ_c for different numbers of scattering encounters. Also indicated is the employed machine precision

n	δ_c (mm)
1	0.0129
2	2.11×10^{-4}
3	3.43×10^{-6}
4	5.60×10^{-8}
5	9.11×10^{-10}
6	1.48×10^{-11}
7	2.41×10^{-13}
8	3.93×10^{-15}
Machine precision	0.22×10^{-15}
9	6.41×10^{-17}

**Fig. 2.** Wave field at a receiver located in the middle of the receiver array

The recorded waves can be separated into the *ballistic wave* and the *coda*². The ballistic wave is the wave that travels more or less along the line of sight from the source to the receiver. This wave is only affected by multiple forward scattering and consists of the early part of the wave train in Fig. 2. The detour of the multiple-scattered waves compared to the un-scattered direct wave is by definition less than a fraction of the wavelength. This means that the waves that comprise the ballistic wave are scattered within the first Fresnel zone. (The concept of the Fresnel zone and its implications are described in great detail by *Kravtsov* [16].) The coda consists of the multiply scattered waves later in the signal. These waves have been scattered in all directions.

² The term “coda” comes from music, where it denotes the closing part of a piece of music.

A critical length scale can be defined for the average perturbation of the locations of the scatterers that leads to a perturbed wave field that is uncorrelated with the unperturbed wave field. The physics of wave propagation for the coda waves and the ballistic wave is fundamentally different because the ballistic wave is mostly sensitive to the average structure of the medium within the first Fresnel zone [10,15]. For this reason, the critical length scale is different for the ballistic wave and for the coda waves. As shown by *Snieder* [15] the critical length scale for the coda waves is given by

$$\delta_c^{\text{coda}} = \frac{\lambda}{4\sqrt{2n}}, \quad (15)$$

while the critical length scale for the ballistic wave is given by

$$\delta_c^{\text{ball}} = \frac{\sqrt{\lambda L}}{\sqrt{12(n+1)}}. \quad (16)$$

In these expressions λ is the wavelength and L is the source–receiver separation as shown in Fig. 1.

For the coda waves the critical length scale is given by the wavelength divided by the square-root of the number of scatterers encountered. Note that in contrast to the critical length scale (13) for the particles the critical length scale for the coda waves does not depend on the scattering cross-section. The reason for this is that for the coda waves the wavelength is the relevant length scale that determines the interference between the multiply scattered waves. For the ballistic wave the critical length scale is proportional to $\sqrt{\lambda L}$. This quantity gives the width of the Fresnel zone in a homogeneous medium [16]. Since the ballistic wave is only sensitive to the properties of the medium averaged over the Fresnel zone, the ballistic wave is only affected when scatterers are moved out of the Fresnel zone when they are displaced. For this reason the width $\sqrt{\lambda L}$ of the Fresnel zone is the relevant scale length for the ballistic wave.

Using (10) the critical length scale for the coda waves can be rewritten as

$$\delta_c^{\text{coda}} = \frac{\lambda}{4\sqrt{2vt/l}}. \quad (17)$$

Note that the time dependence of this quantity is given by $1/\sqrt{t}$, which indicates an algebraic decay of the critical length scale with time. In contrast to this, the time dependence of the critical length scale (14) for the particle scattering decays as $\exp(-\mu t)$, which denotes an exponential decay with time. Since the algebraic decay of (17) implies a much slower decay with time than the exponential decay of the critical length scale of the particles, the wave propagation is much more robust for perturbations of the system than the particle propagation. *Snieder* and *Scales* [14] conjecture that this is due to the fact that the scattered waves travel along all possible trajectories between scatterers and continue to do so when the system is perturbed, whereas the

particles may travel along a fundamentally different path when the scatterer locations are perturbed.

The difference in the time dependence for the wave system and the particle system (algebraic versus exponential) has also been noted for the periodically kicked rotator. In this system a particle (or wave) moves along a ring and is exposed after each time interval T to a kick in a fixed direction. Classically this system displays chaotic behavior and the initial perturbation of the particle along the ring grows exponentially with time. As shown by *Ballantine* and *Zibin* [17] the corresponding quantum system is sensitive to a critical perturbation in the initial angle that varies with time as $1/\sqrt{t}$, which is the same time dependence as in (17). It is striking that two different systems give rise to the same time dependence of the critical length scale for both the particles and the waves.

5 Numerical Examples

In this section numerical examples are used to illustrate the analytical results of Sects. 3 and 4. Let us first consider the time-reversed propagation of particles. When a particle is re-emitted at time $-t$ from the receiver line after its velocity is reversed ($\mathbf{v} \rightarrow -\mathbf{v}$) it should return to the original source position at time $t = 0$. This is illustrated in Fig. 3, where the location of the time-reversed particles is shown at time $t = 0$. In the top panel the location of the particles that are scattered less than or equal to 6 times is shown. In this figure several thousand particles are located at the original source position at $x = z = 0$. The middle panel shows the locations of the particles after time-reversed propagation for the particles that are scattered between 7 and 9 times. Although the particles cluster near the original source position at $x = z = 0$, it can be seen that the particles do not completely converge to this point. The bottom panel shows the location of the time-reversed particles that are scattered 10 or more times. In this case the particles are not concentrated near the original source location at all.

In the numerical simulation of Fig. 3 no explicit errors have been imposed. This implies that the only error is the round-off error of the numerical calculations. The behavior of the time-reversed particles in Fig. 3 can be understood by considering Table 2, where the critical length scale is shown as a function of the number of encountered scatterers. Also shown is the numerical precision of the machine employed to carry out the calculations. When round-off errors are the only source of error, particles that are scattered 6 times or less will refocus on the source after time reversal because the numerical errors are much smaller than the critical length scale (see Table 2). Conversely, the particles that are scattered 10 times or more have according to Table 2 a critical length scale that is much smaller than the round-off error. These particles do not return to the original source position after time reversal. The numerical simulations of Fig. 3 therefore agree well with the results of Table 2.

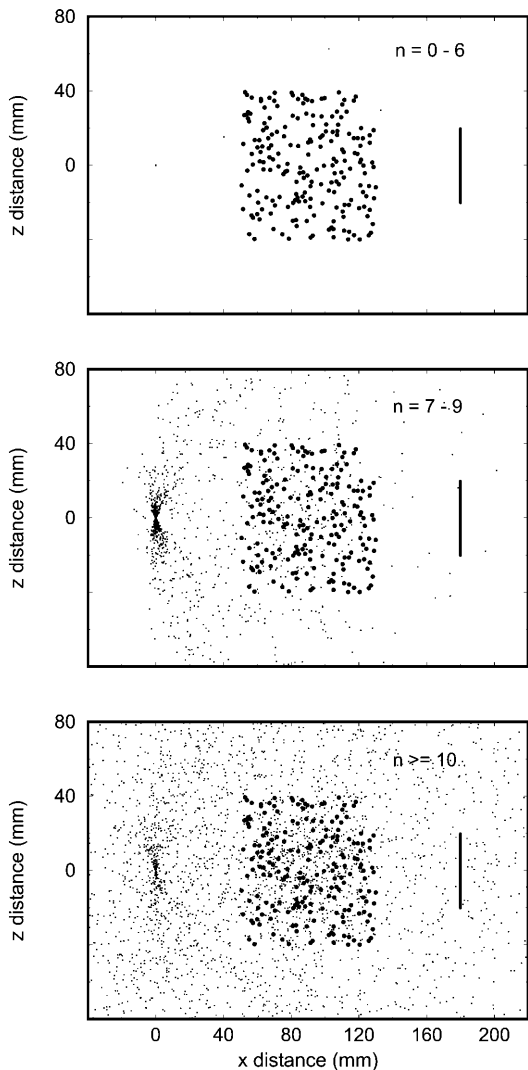


Fig. 3. Locations of the particles (*small dots*) at $t = 0$ after time-reversed propagation for particles that had 6 or less scatterer encounters (*top*), between 7 and 9 scatterer encounters (*middle*) and 10 or more scatterer encounters (*bottom*). In the *top panel* several thousand particles are located at the source position at $x = z = 0$. The original source position is indicated by a *star* in Fig. 1

In the next examples the particles are time-reversed after the scatterer locations have been randomly perturbed. The distance of the time-reversed particles to the source location is a measure of the error in the time-reversed propagation through the perturbed system. This error is converted to a number that measures the quality of the time-reversed propagation by the func-

tion $\exp(-\text{error}/D)$, where “error” is the mean distance of the time-reversed particles from the original source location and D is the typical length scale of the experiment. When all the particles refocus on the source, the error is zero and the exponential is equal to unity, while the function $\exp(-\text{error}/D)$ is much smaller than unity when the particles do not propagate back to the source.

The quality of the time-reversed propagation that is defined in this way is shown in Fig. 4 as a function of the root-mean-square value of the perturbation of the scatterer positions before the reversed propagation. The curves are shown for different numbers, n , of encountered scatterers. Note that the logarithmic scale along the horizontal axis spans 13 orders of magnitude! The critical length scale of (13) is indicated by the vertical arrows. Each of the curves shows a characteristic decay when the error in the scatterer location exceeds a certain critical value. The point at which the quality of the time-reversed propagation degrades agrees well with the critical length scale indicated by the vertical arrows.

The waves that are time-reversed refocus at time $t = 0$ at the original source position through a process of constructive interference. When the system is perturbed before time reversal the height of the interference peak decreases. Thus the ratio of the interference peak at the original source location $x = z = 0$ of the perturbed system to the same corresponding quantity of the unperturbed system is a measure of the accuracy of the time-reversed propagation. When this quantity is equal to unity, the time-reversed prop-

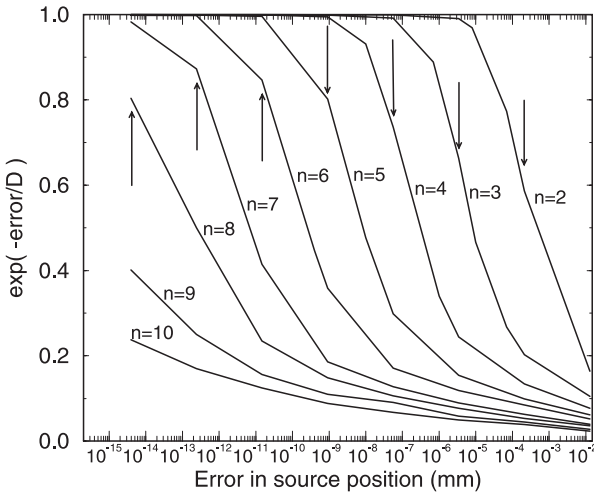


Fig. 4. Imaging quality defined as $\exp(-\text{error}/D)$ as a function of the perturbation of the initial position of the time-reversed particle. The analytical estimates of the the critical perturbation are indicated by *vertical arrows*

agation is optimal, whereas a small value of this quantity denotes degraded time-reversed propagation.

The quality of the time-reversed propagation of the waves that is defined in this way is shown in Fig. 5 both for the ballistic wave (dashed line) and for coda waves that are scattered approximately 10, 20 or 30 times (the solid lines of the left). Details of this numerical experiment are given by *Snieder and Scales* [14]. The analytical estimates of the critical length scales as given in (15) and (16) are shown by the vertical errors. Note that the critical length scales agree well with the numerical simulations.

The solid lines in the middle denote the quality of the time-reversed propagation when the source for the time-reversed propagation is perturbed for the ballistic wave and coda waves in three time intervals. In this case only the wave path from the source to the first scatterer changes; hence the critical length scale is given by $\lambda/4$, and this length scale does not depend on the time interval that is used for the time-reversed propagation [14].

The ballistic wave is much more robust for perturbations of the system than the coda waves. This is due to the fact that the critical length scale for the ballistic wave is given according to (16) given by the width of Fresnel zone, whereas the critical length scale of the coda waves is given according to (15) proportional to the wavelength. Since the width of the Fresnel zone is much larger than the wavelength (with a factor $\sqrt{L/\lambda}$), the critical length

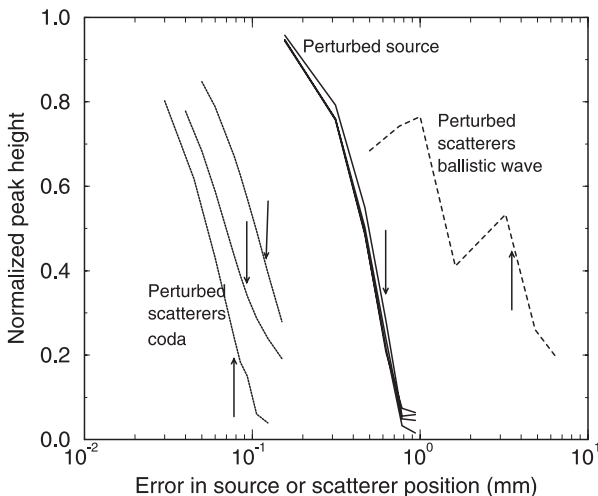


Fig. 5. Quality of time-reversed propagation of waves measured as the ratio of the peak height of the imaged section for the experiment with perturbed conditions compared to the peak height for the unperturbed imaged section. The *dashed line* represents the ballistic wave with perturbed scatterers. The *dotted lines* are for the three coda intervals for perturbed scatterers, with the latest coda interval on the left. The critical length scales from the theory are shown by *vertical arrows*

scale of the ballistic wave is much larger than the critical length scale for the coda waves. In addition, the number of scatterers encountered is much larger for the coda waves than for the ballistic waves. With the factor $1/\sqrt{n}$ in (15) this gives a further reduction of the critical length scale for the coda waves compared to the same quantity for the ballistic wave.

6 Discussion

The most striking feature in a comparison of Figs. 4 and 5 is the scale along the horizontal axis. For the particles the critical scale length ranges between 10^{-15} mm and 10^{-3} mm for particles that are scattered 8 or 2 times respectively. For the waves the critical length scale ranges between 10^{-1} mm and 4 mm for the coda waves that are scattered 30 times and the ballistic wave respectively. This indicates that wave propagation is vastly more robust than the propagation of particles. Mathematically this is related to the fact that the critical length scale decays exponentially with time [$\exp(-\mu t)$] for the particles, while for the waves the critical length scales decay algebraically with time ($1/\sqrt{t}$). Physically there are two reasons that explain this difference. The particles are point-like objects with no scale, whereas the waves are associated with a wavelength. The wave field “feels” its environment on a scale that only depends on the wavelength; hence the wavelength determines a natural scale for the sensitivity of scattered waves for perturbations of the scatterer locations. In addition, the waves travel along all possible scattering paths, whereas the particles each travel along a unique path. When the scatterer locations are perturbed, the waves still travel along all possible scattering paths, whereas a particle may suddenly follow a fundamentally different trajectory. Both effects should form an essential element in accounting for the differences between classical chaos and wave chaos.

References

1. J. Chaiken, R. Chevray, M. Tabor, Q. M. Tan, Experimental study of Lagrangian turbulence in a Stokes flow, Proc. R. Soc. Lond. A **408**, 165–174 (1986) 3
2. K. Popper, The arrow of time, Nature **177**, 538, (1956) 4
3. P. Coveney, R. Highfield, *The Arrow of Time* (Harper Collins, London 1991) 4
4. H. Price, *Time’s Arrow and Archimedes’ Point, New Directions for the Physics of Time* (Oxford Univ. Press, New York 1996) 4
5. A. Derode, P. Roux, M. Fink, Robust acoustic time reversal with high-order multiple scattering, Phys. Rev. Lett. **75**, 4206–4209 (1995) 4, 5
6. A. Derode, A. Tourin, M. Fink, Ultrasonic pulse compression with one-bit time reversal through multiple scattering, J. Appl. Phys. **85**, 6343–6352 (1999) 4
7. J. Scales, R. Snieder, Humility and nonlinearity, Geophysics **62**, 1355–1358 (1997) 4

8. E. N. Lorenz, Deterministic nonperiodic flow, *J. Atmos. Sci.* **20**, 130–141 (1963) [4](#)
9. M. Tabor, *Chaos and Integrability in Nonlinear Dynamics* (Wiley-Interscience, New York 1989) [4](#), [5](#)
10. J. Groenenboom, R. Snieder, Attenuation, dispersion and anisotropy by multiple scattering of transmitted waves through distributions of scatterers, *J. Acoust. Soc. Am.* **98**, 3482–3492 (1995) [5](#), [7](#), [9](#)
11. R. Snieder, A. Lomax, Wavefield smoothing and the effect of rough velocity perturbations on arrival times and amplitudes, *Geophys. J. Int.* **125**, 796–812 (1996) [5](#)
12. M. C. Gutzwiller, *Chaos in Classical and Quantum Mechanics* (Springer, Berlin, Heidelberg 1990) [5](#)
13. J. Scales, R. Snieder, What is a wave?, *Nature* **401**, 739–740 (1999) [6](#)
14. R. Snieder, J. A. Scales, Time reversed imaging as a diagnostic of wave and particle chaos, *Phys. Rev. E* **58**, 5668–5675 (1998) [6](#), [7](#), [9](#), [13](#)
15. R. Snieder, Imaging and averaging in complex media, in J. P. Fouque (Ed.) *Diffuse Waves in Complex Media* (Kluwer, Dordrecht 1999) pp. 405–454 [6](#), [7](#), [9](#)
16. Ya. A. Kravtsov, Rays and caustics as physical objects, *Prog. Opt.*, **XXVI**, 227–348 (1988) [8](#), [9](#)
17. L. E. Ballantine, J. P. Zibin, Classical state sensitivity from quantum mechanics, *Phys. Rev. A* **54**, 3813–3819 (1996) [10](#)

Index

ballistic wave, 8

chaos

– quantum, 5

chaotic, 7

coda, 8

diffusive, 6

Fresnel zone, 8

Lyapunov

– coefficient, 7

– exponent, 4

mean free path, 6

scattering cross-section, 6

time

– reversal, 1

time-reversal

– invariance, 1

time-reversed wavefield, 2

wave

– multiple-scattered, 7